



UKAEA

Preprint



AN EXPERIMENTAL STUDY OF TOKAMAK PLASMAS WITH VERTICALLY ELONGATED CROSS SECTIONS

D C ROBINSON
A J WOOTTON

CULHAM LABORATORY
Abingdon Oxfordshire

1978

This document is intended for publication in a journal or at a conference and is made available on the understanding that extracts or references will not be published prior to publication of the original, without the consent of the authors.

Enquiries about copyright and reproduction should be addressed to the Librarian, UKAEA, Culham Laboratory, Abingdon, Oxfordshire, England

AN EXPERIMENTAL STUDY OF TOKAMAK PLASMAS WITH VERTICALLY ELONGATED CROSS SECTIONS

D. C. Robinson and A. J. Wootton

Culham Laboratory, Abingdon, Oxon, OX 14 3DB, U.K.
(Euratom/UKAEA Fusion Association)

ABSTRACT

The production and equilibrium of tokamak plasmas with vertically elongated cross sections are described. Axisymmetric instabilities, which are controlled by a passive feedback system, restrict the semi axis ratio to less than 1.5. Both the appearance and growth times of these instabilities are theoretically predicted. Poloidal magnetic field oscillations are shown to confirm the plasma shape deduced from equilibrium calculations. The poloidal beta, central electron temperature and overall energy confinement time increase with increasing semi axis ratio.

(Submitted for publication in Nuclear Fusion).

April 1978

INTRODUCTION

This paper describes the results of a series of experiments performed on a small tokamak to investigate effects associated with shaping the plasma cross section [1, 2, 3]. It is generally considered that better plasma parameters can be obtained using a vertically elongated cross section. Gains in total beta $\propto (b/a)^3$ have been suggested, [4] where b is the vertical, and a the horizontal, semi axis length. Limitations imposed by local instabilities can be overcome by a suitable triangular deformation.

The production and equilibrium of the plasma is described, for semi axis ratios between 1.0 and 1.5. Methods of determining the plasma position and shape are discussed. The exact shape, determined by comparing the measured magnetic fields with the fields predicted by a free boundary equilibrium calculation, was elliptic with a smaller triangular deformation. The elongation was limited by the appearance of axisymmetric instabilities. A motion approximating a rigid vertical shift was found, which is predicted by theoretical calculations. These calculations include the effect of induced currents in the resistive vacuum vessel. Passive feedback control was achieved using discrete conductors in place of a complete toroidal shell. Axisymmetric instabilities have also been studied in belt pinches, where stability with $b/a \approx 5 - 10$ is obtained by compressing the plasma against an effective conducting shell [5, 6].

Poloidal field oscillations are accredited to tearing instabilities. For modes originating near the plasma edge, the dependence of the onset time on plasma parameters can be expressed through the edge value of the safety factor, $q(a)$. This is also true for D shaped [7, 8] and rectangular [9] cross sections. A comparison between circular and elliptic cross sections has shown that the same value of $q(a)$, ~ 3 , is suitable for stable operation [10].

Experiments with doublet shapes have required larger values of $q(a)$, because of the peaked plasma current densities produced [11]. Experiments with belt pinches show that $q(a) \sim 3$ is suitable for stable operation with $b/a \leq 10$ [12]. These results show that it is possible to obtain plasmas with the same value of $q(a)$ for a variety of shapes. This allows gains in total beta to be achieved by vertical elongation.

The final measurements described show that the poloidal beta, and overall energy confinement time, τ_E , increase as the plasma is elongated. This increase suggests a scaling $\tau_E \propto b/a$ over the parameter range studied. Comparative confinement experiments have been performed for circles, ellipses and doublets on Doublet II A [10, 11]. Results show increasing density and confinement time with semi axis ratios, but it is not clear whether these gains are directly related to b/a .

MACHINE

The experiments were performed on TOSCA, a small tokamak without a conducting shell^[13]. The conducting vacuum vessel, major radius $R_0 = 30$ cm and minor radius $r_v = 10$ cm, has a penetration time, τ_v , to poloidal magnetic fields of $7 \mu s$, and to toroidal fields of $60 \mu s$. Base pressures of 10^{-7} Torr were achieved, with hydrogen as a working gas.

Outside the vacuum vessel were 16 single turn windings, the primary and shaping windings, illustrated in Figure 1. They could be connected either in series and parallel combinations, or separately, to capacitor banks. These windings induced the plasma current (initiated by a filament), partially provided the equilibrium maintaining field, and controlled the plasma shape. A four series turn vertical field (B_z) winding was also provided to maintain equilibrium. There was no active feedback control of the plasma position.

The toroidal field B_ϕ , produced by 24 single turn coils outside the primary and shaping windings, had a risetime of 2.5 ms and a decay time of 15 ms.

The plasma aperture was restricted by a titanium coated coil former to ≤ 9.2 cm. An adjustable molybdenum limiter at the outer equator also restricted the plasma size, and permitted variable aspect ratios with $R/a \geq 3.4$.

Typical plasma parameters are listed in table 1, together with the diagnostic technique used. A multi coil induction probe was used to measure magnetic field profiles inside the plasma current carrying region. This showed that the plasma current started as a filament, expanding to an approximately flat distribution at the plasma current maximum ($q(a)/q(o) \sim 1.5$). It was at this time that the results were taken. Later in the pulse the profile peaked ($q(a)/q(o) \sim 2.5$).

EQUILIBRIUM

(a) Experiments

The plasma shape was partly determined by the spatial dependence of the confining field. A primary winding was chosen, which minimised the averages $\langle B_z \rangle$ and $\langle |B_R| \rangle$ inside the vacuum vessel; this ensured that the primary winding current did not influence the plasma shape. The vertical field winding produced a field suitable for maintaining a circular plasma in equilibrium. A subset of the 16 primary and shaping windings was then used to distort the plasma cross section. Table 2 lists the individual windings which comprised the three poloidal field systems: the primary, vertical field and shaping windings.

An elliptic cross section was produced by the addition of a quadrupole field to a circular cross section^[14]. The elongation, expressed as the semi axis ratio b/a , can be estimated from a knowledge of the equilibrium maintaining field, produced by the poloidal field systems. The total poloidal field, and decay index $n = -(R/B_z)(\partial B_z/\partial R)$, was evaluated from a knowledge of the winding positions and currents ($B_z \propto R^{-n}$). Assuming an elliptic cross section, produced by a spatially independent decay index, with a uniform plasma current density and parabolic plasma pressure profile:

$$b/a = 1 + \frac{3}{4} \frac{a^2}{R_p^2} \left(\ln \frac{8R_p}{a} - \frac{17}{12} \right) - \frac{a^2}{R_p^2} \left(\ln \frac{8R_p}{a} + \beta_I - 5/4 \right) n \quad (1)$$

where β_I , the poloidal current beta, $= 8\pi \int p dS_\phi / (\mu_0 I_p^2)$, and S_ϕ is the plasma cross section. In the experiment the decay index was varied by changing the ratio of the quadrupole field to the vertical field, or the ratio of the shaping winding current I_s to the plasma current I_p .

Experimental results are shown in Figure 2. Figure 2a shows the ratio I_s/I_p as a function of time. The shaping current is applied 200 μ s after breakdown. The peak value $I_s/I_p = 0.1$ corresponds to $I_s = 1.5$ kA and $I_p = 15$ kA. Figure 2b shows the decay index, deduced from the measured winding currents. A spatial average is used, $\bar{n} = \int n dS_\phi / \int dS_\phi$, because n varied inside the vacuum vessel. Before the shaping current, and its associated quadrupole field is applied, the vertical field winding maintains $\bar{n} = 0.6$. With $I_s/I_p = 0.1$, $\bar{n} = -1.6$. Using equation (1), with β_I measured to be 0.5, the semi axis ratio changes from $b/a = 1.0$ to 1.3.

The plasma shape is characterised by multipole moments of the plasma toroidal current density [15]. These moments can be constructed from measurements of the poloidal field outside the plasma. The first moment is defined to give the displacement Δ_J of the electrical centre from the vacuum vessel centre, and is shown in Figure 2(c). Also shown, as a broken line, is the displacement Δ_R deduced from the B_θ fields measured at the outer and inner equator only ($\theta = 0^\circ$ and 180°). These signals were interpreted to give the displacement of a toroidal filament, with a current equal to the plasma current, at $R = R_0 + \Delta_R$. Both measurements show that the plasma is displaced outwards by the vertical field component produced by the shaping current. Figure 2d shows the second moment, Y_2 , constructed from poloidal field values due to the plasma current. As I_s/I_p increases, and the decay index \bar{n} decreases, then Y_2 decreases. The change in Y_2 associated with the major radial motion shown in Figure 2c is calculated for a filament, and depicted by the broken line in Figure 2d. Therefore the measured decrease in Y_2 is not due to the plasma motion, but reflects a change in plasma cross sectional shape. By representing the plasma as two toroidal filaments, the change in Y_2 can be interpreted as a vertical separation

of 5.3 cm. Alternatively, the change corresponds to an elongation, with $b/a = 1.3$, of a flat current, elliptic plasma ($Y_2 = (b^2 - a^2)/4$).

(b) Computations

The exact plasma shape was determined after comparing the predictions of a free boundary equilibrium calculation with measured parameters [16]. Input data to the calculation consisted of the measured winding and plasma currents, together with the form of the toroidal plasma current $j_\varphi(\psi)$ where $\psi = 2\pi \int_z B_z R dz$. A limiting box was specified, aligned with the limiting apertures within the vacuum vessel, ($Z = \pm 9$ cm, $R = R_0 - 9$ cm, $R_0 + 8.5$ cm) which the plasma boundary touched in at least one place. Both flat ($\partial j_\varphi / \partial \psi = 0$) and peaked current distributions were considered. The flat distributions had a ratio of safety factor at the boundary, $q(a)$, to the centre, $q(0)$, of ~ 1.2 , while the peaked distributions had $q(a)/q(0) \sim 3$. The pressure was expressed as a polynomial expansion in flux ψ : first order for a flat current and second order for a peaked current.

Examples of flux surfaces computed using measured winding currents are shown in Figures 3 and 4. Figure 3 represents a case before the shaping current was initiated. A peaked current distribution gives $\beta_I = 0.4$, as measured. The plasma boundary, represented by the broken line, is approximately circular. The circular vacuum vessel lies inside the square box, which it touches at four points. Figure 4 shows a case computed with $I_s/I_p = 0.14$. A flat plasma current density distribution, with $\beta_I = 0.6$, as measured, results in a semi axis ratio $b/a = 1.6$ for the plasma boundary. There is a small triangular deformation pointing inwards.

The results of a number of computations using experimentally measured winding and plasma currents are represented in figure 5. The semi axis ratio b/a is shown as a function of the shaping to plasma current ratio

I_s/I_p . For each experimental case (fixed I_s/I_p) different points correspond to peaked and flat plasma current distributions, with $\beta_I = 0.5$. Knowing the experimental value of I_s/I_p allows a determination of b/a , which is dependent on the current profile, but not strongly dependent on β_I over the experimentally measured range. For example, the experimental situation illustrated in Figure 2, with $I_s/I_p = 0.1$, corresponds to semi axis ratios between 1.21 and 1.34. If a more exact value is required, a comparison can be made between the measured and predicted multipole moments, which then restricts the permissible elongations.

Plasma displacement was interpreted either from integrated poloidal field measurements [15], or from the B_θ field at two positions only. Figure 6 shows that the latter method of determining the plasma centre is not affected by the elongated cross sections produced. For each free boundary equilibrium computed, the signal

$$S = \left(B_\theta(\theta = 180) - B_\theta(\theta = 0) \right) / \left(B_\theta(\theta = 180) + B_\theta(\theta = 0) \right)$$

was derived from the fields produced by the plasma current. This signal, which is the one experimentally observed, is shown as a function of the displacement of the geometric centre of the plasma boundary, Δ_R . Shown as a solid line is the signal derived for a single toroidal filament, at a position $R_0 + \Delta_R$. Over the range $0 < \beta_I < 1.8$, $0.5 \leq l_i \leq 1.0$ and $1.0 \leq b/a \leq 2.0$, errors in Δ_R resulting from the filament approximation are ≤ 3 mm. Here l_i is the plasma self inductance per unit length, where $l_i = 4\pi \int B_p^2 dS_\phi / (\mu_0 I_p)^2$. Similar results show that the plasma vertical position Δ_Z , can be accurately determined using two coils above and below the plasma ($\theta = 90^\circ$ and $\theta = 270^\circ$), and interpreting the results as being due to the motion of a single filament.

AXISYMMETRIC INSTABILITIES

(a) Experiment

Above a certain value of I_s/I_p , corresponding to a particular decay

index n , or, given the plasma parameters, a semi axis ratio b/a , the plasma was positionally unstable [2, 3]. It was to avoid this instability that the shaping current was applied 200 μ s after the start of the plasma current. Magnetic induction coils around the vacuum vessel showed the plasma to move either up or down ($\pm Z$), depending on whether the initial equilibrium position was displaced up or down by stray major radial fields $B_R(Z=0) \leq 0.05 B_Z(Z=0)$. The motion was independent of toroidal position (l , the wave number in the toroidal direction, $= 0$) the plasma moving approximately as a rigid body (the wave numbers in the poloidal direction being dominated by $m = 1$).

The motion was stabilised by connecting selected pairs of the 16 primary and shaping windings, above and below the plasma, in parallel. These windings, which were previously disconnected, now acted as a passive feedback system; the plasma motion induced currents which acted to restore the plasma to its original position. The critical value of I_s/I_p at which instabilities occurred was determined as a function of aperture (aspect ratio) and passive feedback control.

Figure 7 shows a set of experimental data taken with a full aperture plasma $a(\text{limiter}) = 8.5 \text{ cm}$, $\frac{a}{R_p} \leq 0.3$. Figure 7a shows the volts per turn measured at the top of the vacuum vessel ($\theta = 90^\circ$) both with and without a plasma: also shown are the times when the primary (I_{pr}) vertical field (I_b) and shaping (I_s) winding currents were initiated. Figure 7b and 7c show the plasma current I_p and shaping current I_s . The current in the passive feedback control system is shown in Figure 7d. This system consisted of four windings in two parallel pairs (see table 2): the current shown is that flowing in windings 5 and 12 ($\theta = 101^\circ$ and 259°). Without a plasma there is no current; with the plasma present the current changes with the vertical displacement, which is shown in Figure 7e. Through-

out the vertical motion the horizontal position stays constant, with $R_p = 0.295$ m, as shown in Figure 7f. The two displacement curves, 7e and 7f, are interpreted assuming the plasma to be equivalent to a toroidal filament $R = R_o + \Delta_R$, $Z = \Delta_Z$. The difference between the signals with and without a plasma is proportional to the product $\Delta \times I_p$. This interpretation was justified in the section entitled 'Equilibrium Computations'. Account must be taken of any currents induced by the plasma current itself; for example the currents in the passive feedback windings.

From Figures 7b, 7c, and 7e, it is concluded that the plasma centre starts to move, exponentially in time, downwards when I_s/I_p reaches ~ 0.2 , this is the axisymmetric instability. The plasma area is reduced and the current density increases, so that the safety factor is reduced. A disruption results, seen in figure 7a, as a negative voltage spike, and the plasma current is terminated.

The growth time τ was measured as a function of the ratio I_s/I_p . The growth time was deduced from the time derivative of $\ln(\Delta_Z)$ with Δ_Z between 2 mm and 5 mm; the ratio I_s/I_p was derived at the time corresponding to a displacement of $\Delta_Z = 3.5$ mm.

Figure 8 and 9 show the results obtained with and without passive feedback control, for both full aperture plasmas ($R/a \geq 3.4$) and reduced aperture plasmas ($R/a \geq 6$). With a full aperture plasma, Figure 8 shows that $I_s/I_p \leq 0.04$ for stability without control (marked A), and $I_s/I_p \leq 0.17$ for stability with control (marked B). As the ratio I_s/I_p is increased, the growth time τ decreases, approaching the vacuum vessel penetration time $\tau_v = 7 \mu s$. Figure 9 shows similar results for a reduced aperture plasma. Here $I_s/I_p < 0.035$ for stability without control (marked A) and ≤ 0.055

for stability with control (marked B). The critical value of I_s/I_p without control (A) is approximately independent of the aspect ratio, but the critical value with control, (B) is three times as large for the full aperture plasma as for the reduced aperture plasma.

Using Figure 5, the critical values of I_s/I_p derived from Figure 8 can be related to semi axis ratios of the plasma cross section. Without passive control windings, $b/a \leq 1.1$ for stability: with control $b/a \leq 1.5$. For reduced aperture plasmas, curves similar to those in Figure 5 were computed. For a given value of I_s/I_p , reducing the aperture (increasing the aspect ratio) reduced the semi axis ratio. The critical values of I_s/I_p in Figure 9 correspond to the computed values $b/a < 1.05$ without control and $b/a < 1.15$ with control. No dependence on the edge value of safety factor, $q(a)$, was observed, with either a full or reduced aperture.

(b) Calculations

Energy principle calculations have been performed for non-circular cross sectioned plasmas. Calculations assuming both skin current [17] and flat current [18] equilibria show that for ellipses the most unstable perturbation is a rigid shift. However, cross sections with triangular and rectangular deformations are more unstable than is predicted by this trial function, although the largest component of the motion is still the rigid shift. The non-elliptic component of the experimental plasma outer boundary, derived from the free boundary equilibrium calculations, is small, so that a rigid shift trial function can be assumed (measured multipole moments give the ratio $a_p Y_2/Y_3$, characterising ellipticity/triangularity, ~ 8).

A displacement in the vertical direction results in a force acting on the plasma $\int \bar{j}_\phi \times \bar{B}_R dV$ where j_ϕ is the plasma toroidal current density. By representing the plasma as a filament, and relating the field B_R to the

decay index n , the stability criterion can be expressed as $n > 0$. This criteria is also valid with more realistic assumptions [19].

The conducting vacuum vessel acts as a resistive shell, with the induced currents determining the growth rate of the instability [20]. Assuming a rigid shift, a small non circular distortion of the cross section, and a slowly growing mode compared to Alfvén transit times, the growth time can be expressed as

$$\tau = \tau_v \frac{2R^2}{\Lambda r_v^2 n}$$

$$\text{where } \Lambda \equiv \ln \frac{8R}{a} + \beta_I + \frac{1}{2} - 3/2 = \frac{4\pi B_Z R}{\mu_0 I_p} \quad (2)$$

In Figure 8 and 9 this analytic dependence is shown as a solid curve, and predicts the experimentally determined times with no passive feedback control.

To determine the stabilising influence of the control system a rigid shift was again assumed, the induced currents in the parallel connected windings derived, and the volume force acting on the plasma, either stabilising or destabilising, evaluated [21]. It was assumed that both the plasma and parallel connected windings were perfectly conducting. A specified equilibrium plasma current distribution was represented by a number of toroidal filaments. The currents in a set of discrete conductors outside the plasma, a virtual shell, were chosen to make the plasma surface a flux surface: the specified plasma shape and current distribution were then in equilibrium. Each filament was displaced equally, keeping the flux constant at each point inside the plasma. The currents in the virtual shell were also held constant. The force acting on the plasma, $F_D = \int \bar{B}_R \times \bar{J}_\phi dV$, was evaluated, where the field B_R resulted from the virtual shell currents. Figure 10 shows the force F_D as a function of the semi axis ratio b/a for a flat current plasma with elliptic cross

section, and $\beta_I = 0$. Two curves are shown, with the geometric constraints 1) $b = 9$ cm and 2) $a = 4.5$ cm, corresponding to the full and reduced aperture experiments.

Stability corresponds to $F_D < 0$: that is $b/a < 1.08$ for a full aperture plasma (case 1) and $b/a < 1.05$ for a reduced aperture plasma (case 2). Both these points correspond to maintaining fields with $n = 0$. All forces are normalised to the force F_0 acting on a displaced, straight filament inside a perfectly conducting cylindrical shell, radius 13 cm.

The stabilising influence of the passive feedback control windings is also evaluated. The plasma displacement induced currents in these additional windings which depended on both the mutual and self inductances. The resulting additional field, B_R , produced a stabilising force $F_S = \int \bar{B}_R \times j\varphi \, dV$. This is shown in Figure 10, as $-F_S$. Stability corresponds to $F_D + F_S < 0$: i.e. $b/a < 1.5$ for a full aperture plasma and $b/a < 1.15$ for a reduced aperture plasma. The experimentally determined limits are marked on the figure, and are in good agreement with the curves shown. Table 3 summarises the results.

Also shown in Figure 10 is the stabilising force produced, had all sixteen primary and shaping windings, connected in parallel, been available for control. The result would allow $b/a \leq 1.6$. A complete toroidal shell at the conductor positions would allow $b/a \leq 1.8$ [22].

Calculations have also been performed with a peaked plasma current, giving similar results to those presented with the flat current (Figure 10); which distribution is the more unstable depends on the aspect ratio.

These calculations assumed perfectly conducting windings. Including a finite winding resistance will give the original stability criteria, $n > 0$ [23], or $b/a < 1.1$, for a full aperture plasma in TOSCA. However, between the values of $b/a = 1.1$ and 1.5 (or 1.05 and 1.15 for a reduced aperture plasma)

the growth time will be given by a formula similar to equation 2, with the vacuum vessel penetration time replaced by the winding current decay time. The expected growth times are then ~ 20 ms, outside the experimental observation time, so that the plasma appears stable. For times longer than 20 ms active feedback control would be required.

KINK MODE STABILITY

Oscillations of the poloidal magnetic field have been observed with magnetic induction coils, and can be assigned a poloidal and toroidal mode number, m and l . Modes with $m = 5, 4, 3$ and 2 , and $l = 1$ were detected. Magnetic induction coils have also been inserted into the plasma current carrying region. For distances of up to 2 cm this probe did not affect the observed plasma parameters, or the structure of the poloidal field oscillations measured at the vacuum vessel. The B_r signal, measured across the integer q surface near the plasma edge, was single signed, implying that the field perturbation was due to a resistive mode [24]. Estimates for resistive interchange modes showed them to be stable, [25] suggesting that the perturbations were due to tearing modes. Such oscillations are caused by magnetic structures (islands) rotating in the direction of the electron diamagnetic drift [26].

The onset time of oscillations was related to the plasma parameters at this time [7, 8], in particular to the shaping current. Figure 11 shows curves of I_s/I_p as a function of time for four different discharges (including $I_s/I_p = 0$). The appearance of the $m = 4, l = 1$ oscillation is marked by hatching. Assuming that the $m = 4$ oscillation originates from the plasma edge, with $q = m/l$, then

$$q = \frac{m}{l} = \frac{2\pi a^2 B_\phi}{\mu_0 I_p R_p} \left(\frac{1 + b^2/a^2}{2} \right) \quad (3)$$

If it is assumed that the vertical dimension b is limited geometrically to 8.5 cm, the semi axis ratio can be deduced at the mode onset time. This is shown in Figure 12 as a function of the ratio I_s/I_p at the mode onset time.

Also reproduced are the two curves representing the equilibrium calculation values of b/a , for a given I_s/I_p , for both flat and peaked plasma current density distributions (Figure 5). The values of b/a deduced from the mode analysis agree with those derived from equilibrium theory. This suggests that the influence of the shaping on the tearing modes is expressed through the safety factor alone, as was assumed in the analysis. The same result was found for the $m = 3$ oscillations.

Tearing modes are predicted theoretically to appear only when $q(a) > m/l$. This implies that the values of b/a deduced from the mode analysis, shown in Figure 11, are the minimum ones. This is consistent with the fact that the curve for a flat plasma current density predicts large b/a values. If the plasma is defined by a separatrix, rather than by the limiter, equation (3) is not applicable, and $q(a) \rightarrow \infty$. However, equation (3) still represents the safety factor at small distances from the separatrix, so that the values of b/a would be approximately correct.

CONFINEMENT PROPERTIES

Toroidal flux loops have been used to measure the poloidal beta value. The plasma energy input, determined from the current and volts per turn, allows the energy confinement time to be derived. Laser light scattering was used to measure the central electron temperature. Results of these measurements are presented as functions of the plasma semi axis ratio.

Two sets of toroidal flux loops, inside and outside the vacuum vessel, were used to determine the flux $\Delta\phi = \int (B_\phi - B_{\phi E}) dS_\phi$, where $B_{\phi E}$ is the toroidal field outside the plasma. Average values of $\Delta\phi$ were obtained from both sets of loops, with the plasma current in both directions. Typical deviations from the average were less than 20%. The poloidal current beta was then calculated using $\beta_I = S_1 - \mu_I$ with $\mu_I = 8\pi B_\phi \Delta\phi / (\mu_0^2 I_p^2)$, and S_1 an integral of products

of the poloidal magnetic field components outside the plasma^[27]. This integral was approximated experimentally using B_θ and B_r measurements at the vacuum vessel, and also derived from the free boundary equilibrium calculations. For circular plasmas $S_1 = 1$; for vertical ellipses which $b/a = 1.5$, $S_1 \approx 0.9$.

Experimental results are shown in Figure 13. The plasma current I_p and shaping current I_s result in the ratio I_s/I_p shown in Figure 13a. Figure 13b shows the flux $\Delta\phi$ measured with the toroidal flux loops inside the vacuum vessel, and figure 13c shows β_I , with the correction for the plasma shape, $S_1 < 1$, applied. Also shown as a broken line are results when no shaping current was applied. It is seen that β_I increases when the plasma is shaped, and continues to increase after the maximum of the shaping current, when the cross section is most distorted ($b/a \approx 1.5$). Keeping $q(a)$ and B_ϕ fixed the average value of total beta was increased by approximately 20%.

Laser light scattering measurements showed that this increase in β_I was accompanied by a similar increase in the central electron temperature. Interferometer measurements through the centre and edge of the plasma suggested that the density profile remained a fixed function of the flux ψ .

The plasma energy confinement time τ_E was deduced from a balance between the Ohmic input power and the energy losses. Corrections for time dependent plasma energy ($\beta_I I_p^2$) can be made. The Ohmic input power can be determined from a knowledge of the plasma inductance, and the azimuthally distributed volts per turn, $V(\theta)$ and poloidal field $B_\theta(\theta)$. The inductance can be determined from the azimuthally distributed poloidal field, $B_\theta(\theta)$, and the poloidal beta, β_I ^[27]. In this way corrections for plasma shape and toroidicity were made. Results are shown in Figure 14, where the energy confinement time is plotted as a function of the semi axis ratio b/a . The semi axis ratio is deduced using Figure 5, and a curve intermediate between those drawn, in order to approximate

the measured plasma current distribution ($q(a)/q(0) \sim 1.5$). Results are shown for vertical and horizontal ellipses, where the shaping current direction was reversed [3, 28]. If we assume that the energy confinement time depends on the aspect ratio and the elongation with a power law dependence then the results are consistent with the time being independent of aspect ratio but linearly dependent upon the elongation b/a . These results were obtained with approximately constant Ohmic input power.

The possible reasons for the improved confinement times, following the reduced losses, are now discussed. The four loss mechanisms are radiation, charge exchange, convection and conduction. Bolometer measurements show that $\leq 30\%$ of the Ohmic input power is lost by radiation and charge exchange and this is not changed by shaping the plasma cross section. This level is consistent with the measured oxygen impurity lines and the resistance anomaly factor, inferred from an assumed temperature profile, is ≤ 3 . Because the plasma resistance remains constant when the plasma is elongated, the increased central temperature and decreased cross sectional area suggest that the anomaly factor remains constant.

Because the bolometer measurements show that the power lost by radiation and charge exchange is not affected by the shaping, the increased confinement times must be caused by a reduction in either the convection or conduction losses, or both. Neither loss has been separately measured. The shape of the computed flux surfaces outside the plasma edge suggest that, whereas circular surfaces allow cross field losses, the elliptic surfaces intersect the vessel wall. This could lead to worse confinement for ellipses than circles. Also if the confinement times are determined by a spatially independent conduction or diffusion coefficient, the elliptic geometry would reduce the confinement times. This is because the confinement time increases with the ratio of the plasma cross section area to the cross section perimeter, a maximum

for a circular cross section. Therefore the conduction, or diffusion, coefficient must be a decreasing function of b/a .

Fluctuation amplitudes and frequencies may characterise the energy loss process. In the TOSCA experiment magnetic coils show large $m = 2$, $l = 1$ oscillations, probably due to tearing modes. However, the amplitude of these oscillations, measured at the vacuum vessel, was not changed by the elongation in the vertical direction.

The present experiments have not allowed us to determine which mechanism is responsible for the improved confinement.

CONCLUSIONS

Tokamak plasmas with approximately elliptic cross sections have been produced, using discrete conductors. The limit to the elongation was set by the appearance of axisymmetric, or positional instabilities, which terminated the plasma current. With no feedback control, semi axis ratios $b/a < 1.1$ were possible. Using four windings as a passive feedback system, at a distance of ~ 1.5 times the plasma radius from the plasma centre, $b/a \leq 1.5$ was possible for times ~ 2 ms (the experimental observation time). These maximum values of semi axis ratio were reduced as the plasma aspect ratio was increased. Both the appearance and growth times are in good agreement with force calculations which include the effect of induced currents in the windings.

Poloidal field oscillations are accredited to tearing instabilities. The onset time of these oscillations, with poloidal mode numbers 4 and 3, was dependent on the shape only through the safety factor. This permitted shaped and circular plasmas to operate at the same edge value of safety factor, which would result in higher beta values for a constant plasma volume.

Both the poloidal beta, and central electron temperature, were measured to increase with the semi axis ratio, when the Ohmic input power was approximately constant. The energy confinement time was also measured to increase with vertically elongated cross sections. The total beta value increased by approximately 20%.

ACKNOWLEDGEMENTS.

We would like to thank G. Cima for his help during the early phase of these measurements, C. L. Thomas for assisting with the equilibrium calculations and C. Gowers and P. Jones for the laser light scattering measurements.

REFERENCES

1. G Cima, C W Gowers, G E S Harding, R E King, H Krause, D C Robinson P A Wolfe, A J Wootton. Proc. Seventh European Conference on Controlled Fusion and Plasma Physics, Lausaune, 1, 6, (1975).
2. G Cima, D C Robinson, C L Thomas, A J Wootton in Plasma Physics and Controlled Nuclear Fusion Research (Proc. 6th Int. Conf. Berchestgaden, 1976). I.A.E.A., Vienna. 1(1977)335.
3. A J Wootton, D C Robinson, Proc. Eighth European Conference on Controlled Fusion and Plasma Physics, Prague. 1, 42 (1977).
4. E B Kadomtsev. Comments on Plasma Physics and Controlled Fusion, 2, 75 (1976).
5. F Hofmann, L Bighed, J M Peiry, A Simik, in Plasma Physics and Controlled Nuclear Fusion Research. (Proc. 6th Int. Conf. Berchestgaden, 1976) I.A.E.A., Vienna. 1(1977)305.
6. E Graffmann, F Hoenen, A Kaleck, L Koren, M Korten, J Schluter. Eighth European Conference on Controlled Fusion and Plasma Physics, Prague, 1, 77 (1977).
7. A V Bortnikov, N N Brevnov, S N Gerusimov, V C Zhukovskii, V I Pergament, L N Khimchenko. Fizika Plazmy. 1, 931 (1975).
8. H Toyama, K Makishima, H Karneko, M Noguchi, S Yoshikawa, Phys. Rev. Letts., 37, 18 (1976).
9. T. Okuda, Y Tonaka, K Sakurai, K Nakamura. Proc. Eighth European Conference on Controlled Fusion and Plasma Physics, Prague. 1, 121 (1977)
10. R L Freeman et al. General Atomic Report GA-A 13781, A Comparison of circular and elliptic plasma in a doublet IIA. (1976).
11. R. L. Freeman et al, in Plasma Physics and Controlled Nuclear Fusion Research (Proc. 6th Int. Conf. Berchestgaden, 1, 317 (1976).
R K Fuller et al. Phys. Rev. Letts. 39, 623 (1977).
12. O Gruber, R Wilhelm. Nuclear Fusion, 16, 243 (1976).
13. R E King, A J Wootton, D C Robinson. Eighth Symposium on Fusion Technology Conference, 57 (1974).
14. V S Mukhovatov, V D Shafranov. Nuclear Fusion, 11, 605 (1971).
15. L E Zakharov, V D Shafranov. Sov. Phys. Tech. Phys., 18, 151 (1973).
16. C. L. Thomas. Computational Methods in Classical and Quantum Physics (Advanced Publications Ltd.) London (1976).
17. E Rebhan, A Salat. Nuclear Fusion, 17, 251 (1977)
18. M S Chu, R L Miller. General Atomic Report G.A.A.14323. 'Wall stabilisation of axisymmetric modes in non-circular tokamak plasmas'. (1977).
19. F A Hass, J C B Papaloizou, Nuclear Fusion, 17, 721 (1977).
20. A Fukuyama, S Seki, H Momota, R Itatani, Japanese Journal of Applied Physics, 14, 871 (1975).

21. M Okabayashi, G Sheffield. Nuclear Fusion, 14, 263, (1974).
22. F A Haas, Nuclear Fusion, 15, 457 (1975).
23. D Pfirsch, H Tasso. Nuclear Fusion, 11, 259 (1971).
24. J E Crow, J Killeen, D C Robinson. Proc. Sixth European Conference on Controlled Fusion and Plasma Physics, Moscow. 1, 269 (1973).
25. B J Green and H P Zehrfeld. Nuclear Fusion, 17, 1133 (1977).
26. D C Robinson, Bulletin of the APS. 22, 1202 (1977).
27. V D Shafranov. Plasma Physics, 13, 757 (1971).
28. A J Wootton. Accepted for publication in Nuclear Fusion.

TABLE 1

PLASMA PARAMETERS

Geometric: $20.8 \text{ cm} \leq R \leq 38.5 \text{ cm}$
 $a_{\text{p max}} = 8.6 \text{ cm}$ if $R_{\text{p}} = 29.4 \text{ cm}$
 $b_{\text{limiter}} = 9.2 \text{ cm}$

Measured and derived values at peak plasma current:

τ Current Rise $\sim 400 \mu\text{s}$

τ Current Duration $\sim 2 \text{ ms}$

$I_{\text{p}} \sim 15 \text{ kA}$

$V_{\text{p}} \sim 5\text{V}$

$B_{\phi} \sim 0.5 \text{ T}$

$q_{\text{a}} \sim 3-4$

$\beta_{\text{I}} \sim 0.5$

$\frac{1}{2a} \int n_{\text{e}} dl \sim 1-3 \times 10^{19} \text{ m}^{-3}$

T_{e} (Scattering) $\sim 200 \text{ eV}$

Resistance $\sim 0.3 \text{ m}\Omega$

$\tau_{\text{E}} \sim 300 \mu\text{s}$

τ Skin $\sim 300 \mu\text{s}$

$T_{\sigma} \sim 30 \text{ eV}$

T Diamagnetic $\sim 100 \text{ eV}$

T_{i} (Scaled) $\sim 60 \text{ eV}$

Z Effective (Assumed Profiles) ~ 3

τ Equipartition $\sim 300 \mu\text{s}$

TABLE 2
THE POLOIDAL FIELD

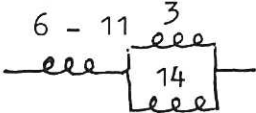


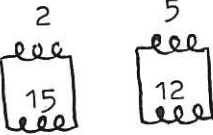
| <u>System</u> | <u>Winding Number (Fig.1.)</u> | <u>Circuit</u> |
|--------------------|---|--|
| Primary | 6,7,8,9,10,11,3,14 ($B_z, B_R \sim 0$) |  |
| Vertical Field | $B_{z1}, B_{z2}, B_{z3}, B_{z4}$ | $B_{z1} - B_{z4}$  |
| Shaping | 1,16,4,13. (nett turns zero) | $1 \quad 16 \quad 4 \quad 13$  |
| Passive Control | 2,15,5,12 (and 3, 14 in primary) |  |

TABLE 3

The axisymmetric stability limits

| | No Control | | With Control | |
|---------------------------------|------------|--------|--------------|--------|
| | experiment | theory | experiment | theory |
| full aperture, $b/a \leq$ | 1.1 | 1.08 | 1.5 | 1.5 |
| reduced aperture, $b/a \leq$ | 1.05 | 1.05 | 1.15 | 1.15 |

The maximum values for stability are quoted.

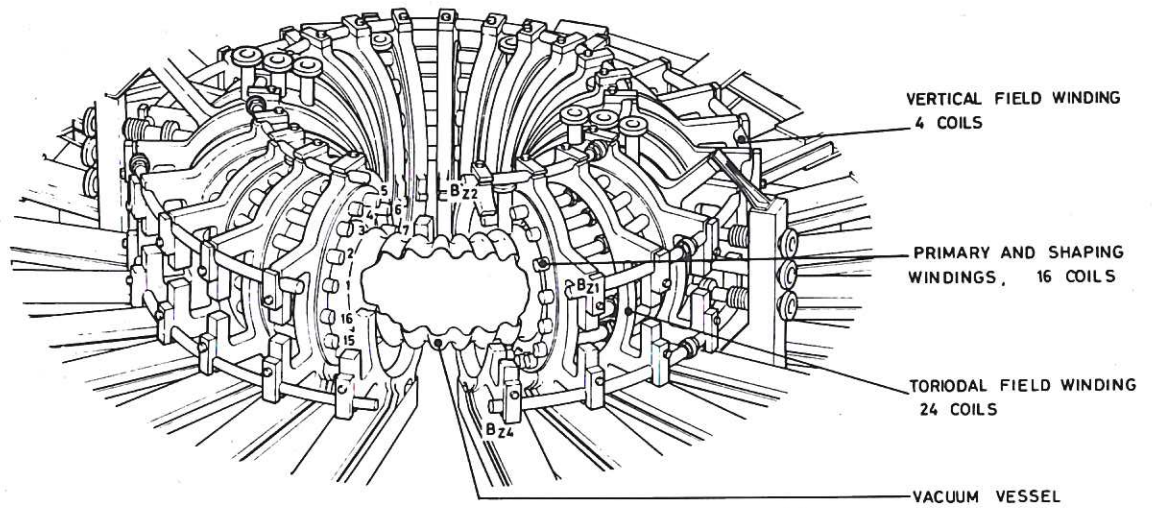
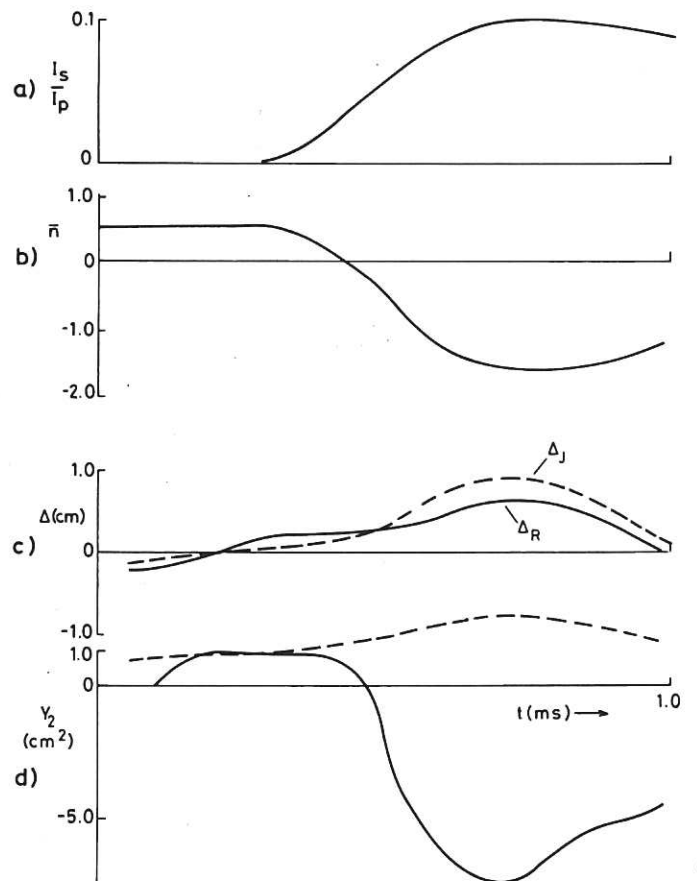


Fig.1 A schematic diagram of the vacuum vessel and windings, showing the principle diagnostics available. The primary windings are shown numbered 1 to 16.

Fig.2 Data from a vertically elongated plasma: (a) I_s/I_p , the ratio of shaping to plasma current; (b) the averaged decay index \bar{n} ; (c) the displacement in the horizontal (major radial) direction. The solid line represents Δ_R , the broken line Δ_J ; (d) the second multiple moment Y_2 . The solid line is that measured experimentally, the broken line that computed for a filament at $R = R_0 + \Delta_R$.



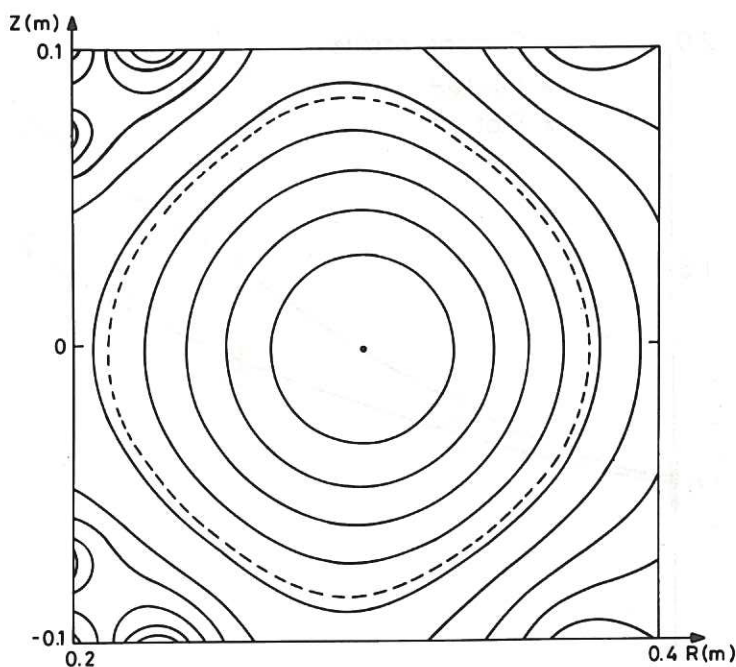


Fig.3 Flux contours computed with measured winding currents: a primary current of 6.57kA, a vertical field winding current of 4.3kA and a plasma current - 16kA. No shaping current was applied. The broken line represents the plasma boundary. A flux dependent plasma current distribution gives $\beta_I = 0.4$, as measured.

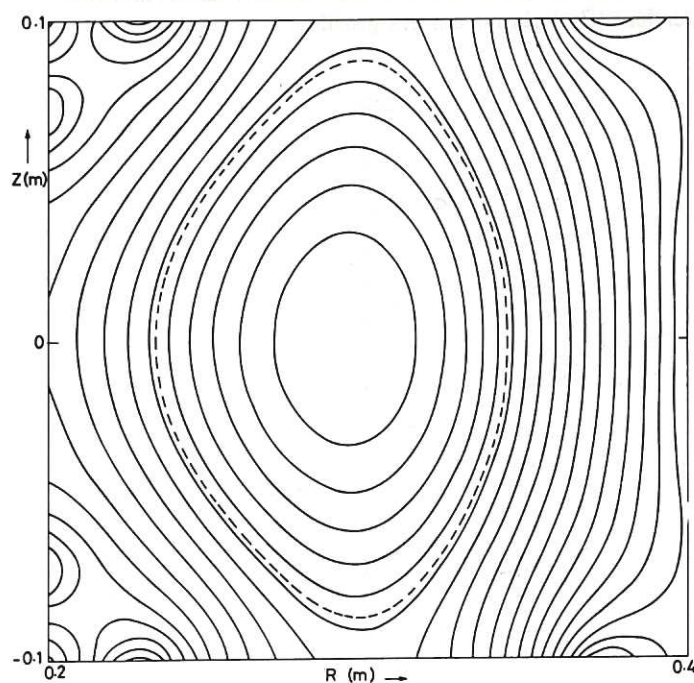


Fig.4 Flux contours computed for a shaped plasma, using measured winding currents: a primary current of 7.5kA, a vertical field winding current of 2.77kA, and a shaping current of 2kA. The plasma current is - 14.3kA. A flux independent plasma current distribution gives $\beta_I = 0.6$, as measured.

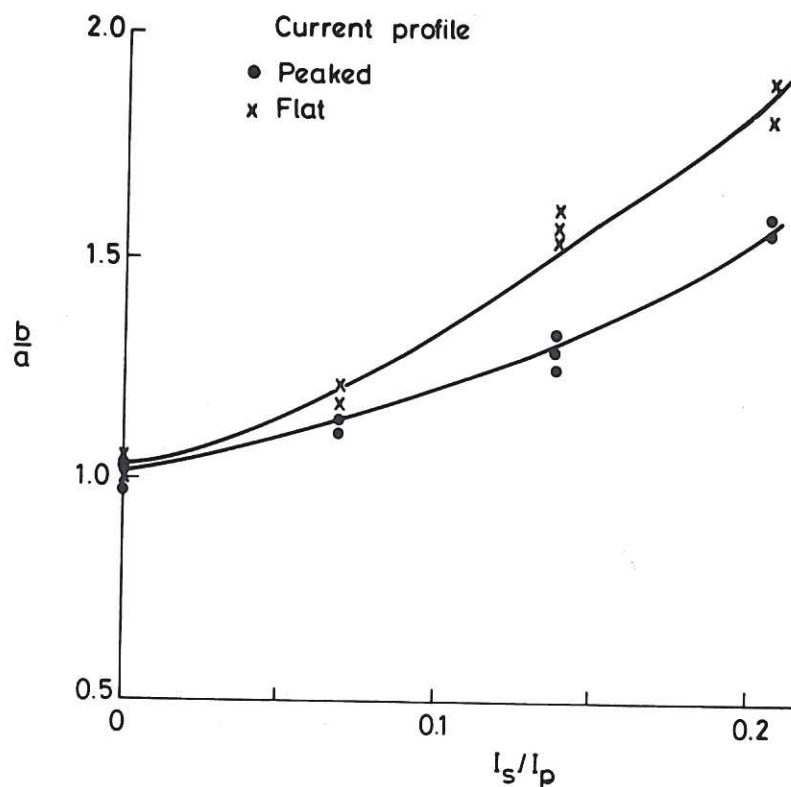


Fig.5 The dependence of the semi-axis ratio of the plasma boundary, b/a , on the ratio of shaping to plasma current, I_s/I_p , deduced from the free boundary equilibrium calculations. In all cases $I_p \sim 15\text{kA}$, and $\beta_I \sim 0.5$. Cases are shown for flux dependent (peaked) and flux independent (flat) plasma current profiles.

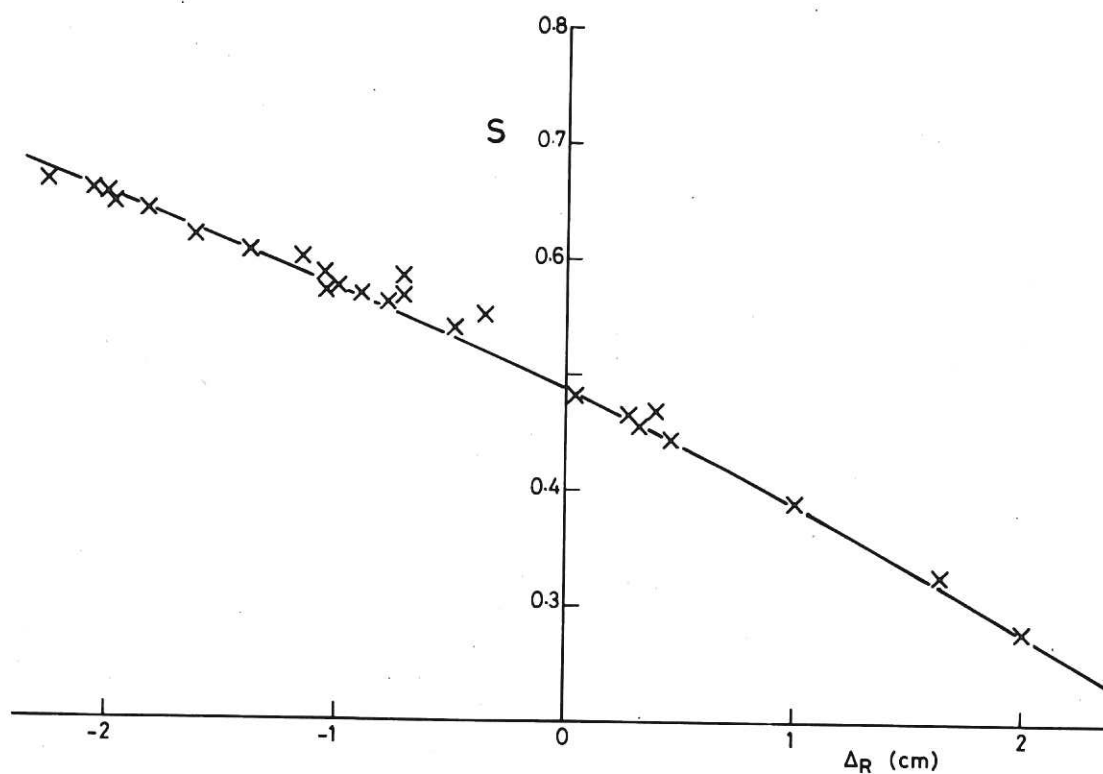


Fig.6 The dependence of $S = (B_\theta(\theta = 180) - B_\theta(\theta = 0)) / (B_\theta(\theta = 180) + B_\theta(\theta = 0))$ on the geometric displacement Δ_R from the centre of the vacuum vessel. Free boundary calculation (crosses) and a filament approximation (line) results are shown.

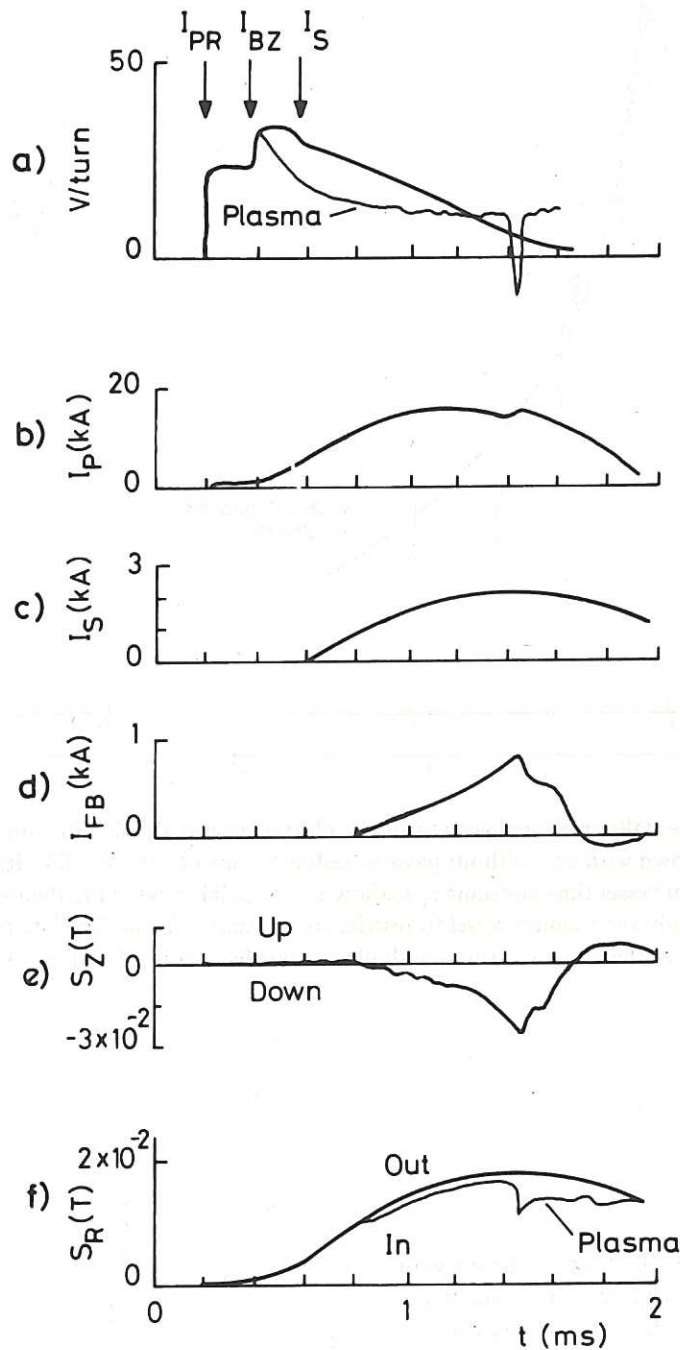


Fig.7 Experimental data on axisymmetric instabilities: (a) the volts per turn at $\theta = 90^\circ$, showing the start times of the primary (I_e), vertical field (I_{bv}) and shaping (I_s) winding currents; (b) the plasma current; (c) the shaping current; (d) the plasma feedback control winding current; (e) the vertical displacement monitor signal; (f) the horizontal displacement monitor signal. Results are shown with and without a plasma.

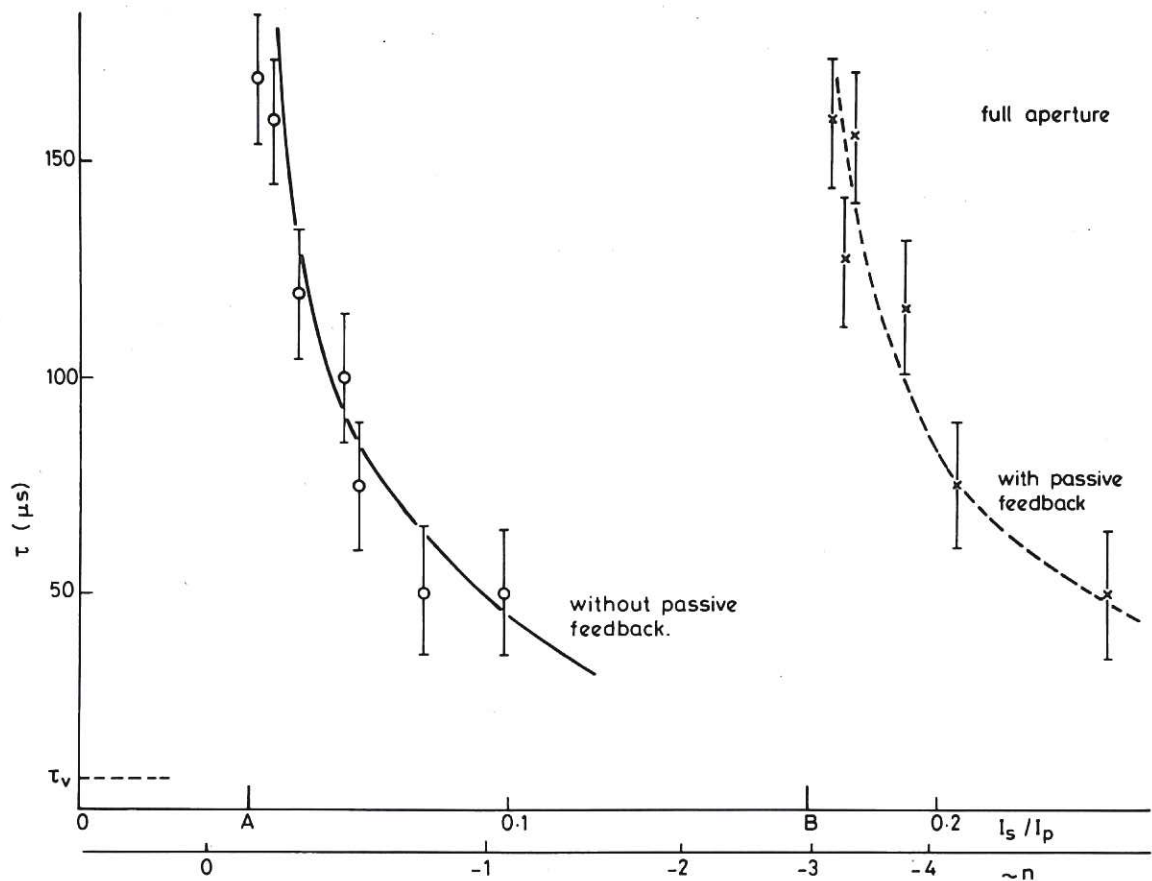
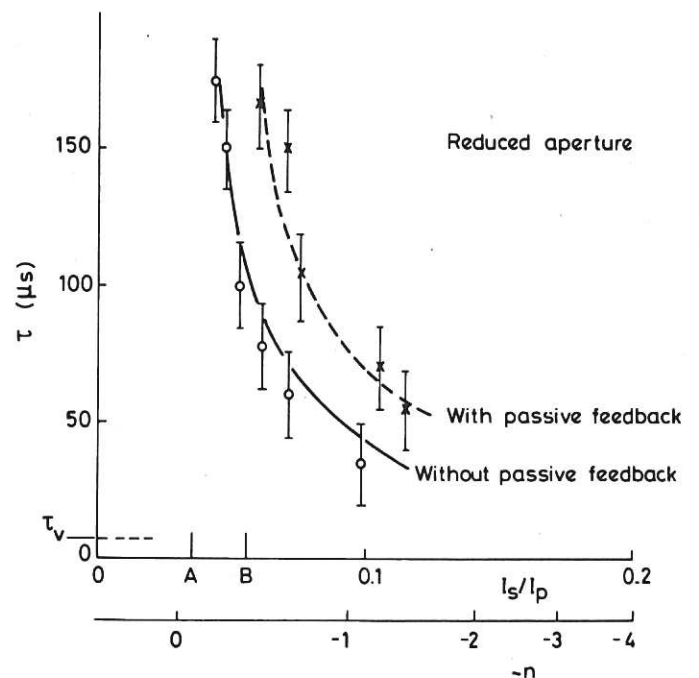


Fig.8 The experimentally measured growth time τ plotted against the shaping to plasma current ratio, I_s/I_p . Cases are shown with and without passive feedback control: the stability limits are marked B and A. The vacuum vessel time constant τ_v is shown. The solid curve is the theoretically predicted dependence with only the vacuum vessel to restrict the motion. The broken line represents a similar dependence, fitted to the measured times with plasma feedback control. All results are with a full aperture plasma.

Fig.9 The experimentally measured growth time τ with a reduced aperture plasma plotted against the shaping to plasma current ratio, I_s/I_p . Cases are shown with and without passive feedback control, the stability limits marked A without control and B with control. The vacuum vessel time constant τ_v is marked. The solid curve is the theoretically predicted dependence with only the vacuum vessel to restrict the motion. The broken line represents a similar dependence fitted to the measured times with passive feedback control.



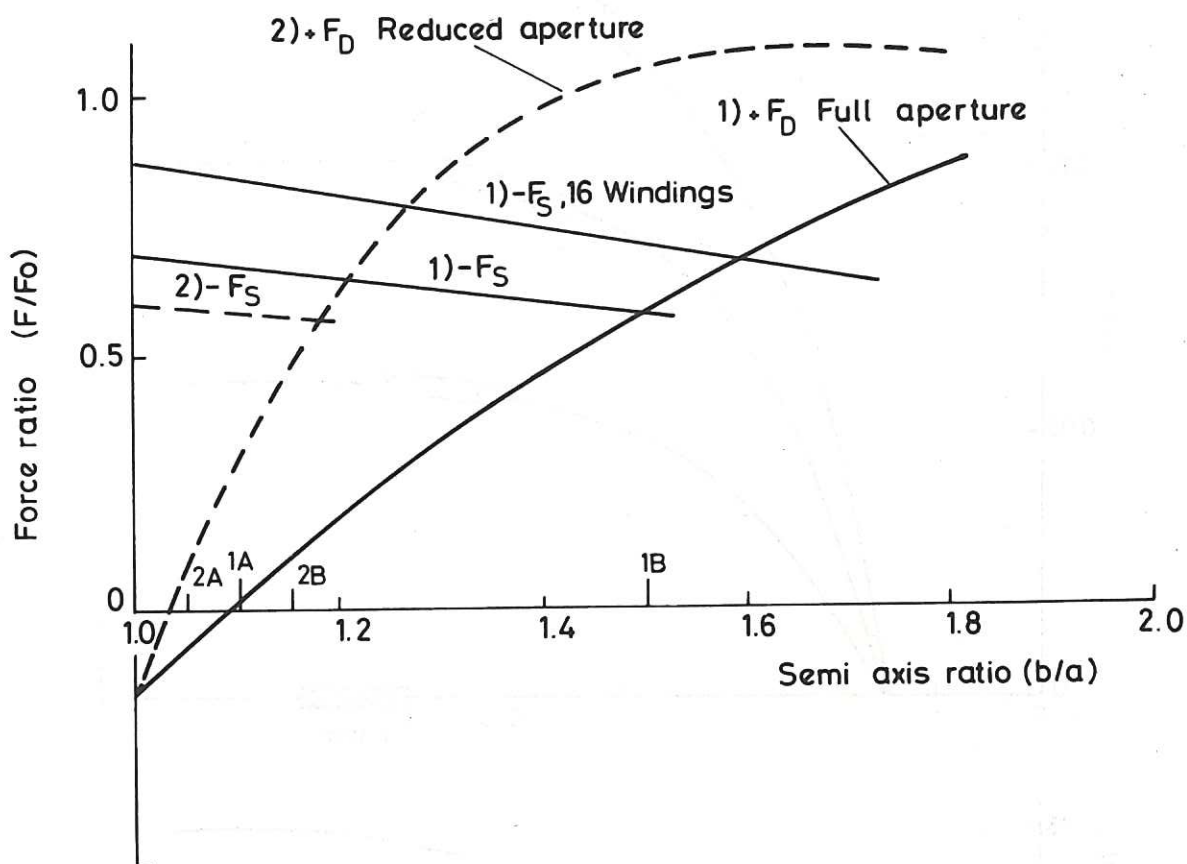


Fig.10 The destabilising force F_D acting on a displaced conductor of elliptic cross-section, initially in equilibrium, as a function of the semi-axis ratio b/a . Curves are shown with two geometric constraints: (1) $b = 9$ cm, $R_0 = 29$ cm and (2) $a = 4.5$ cm, $R_0 = 30$ cm. The restoring force F_S produced by connecting windings 2 and 15, 3 and 14, and 5 and 12 in parallel is also shown for the two cases. The restoring force resulting from all 16 primary windings, acting as a complete shell, is shown for case (1). All forces are normalised to the stabilising force F_0 acting on a displaced filament inside a perfectly conducting shell of minor radius 13 cm. The experimentally determined stability limits are noted: (2A) reduced aperture, no control; (1A) full aperture, no control; (2B) reduced aperture with control; and (1B) full aperture with control.

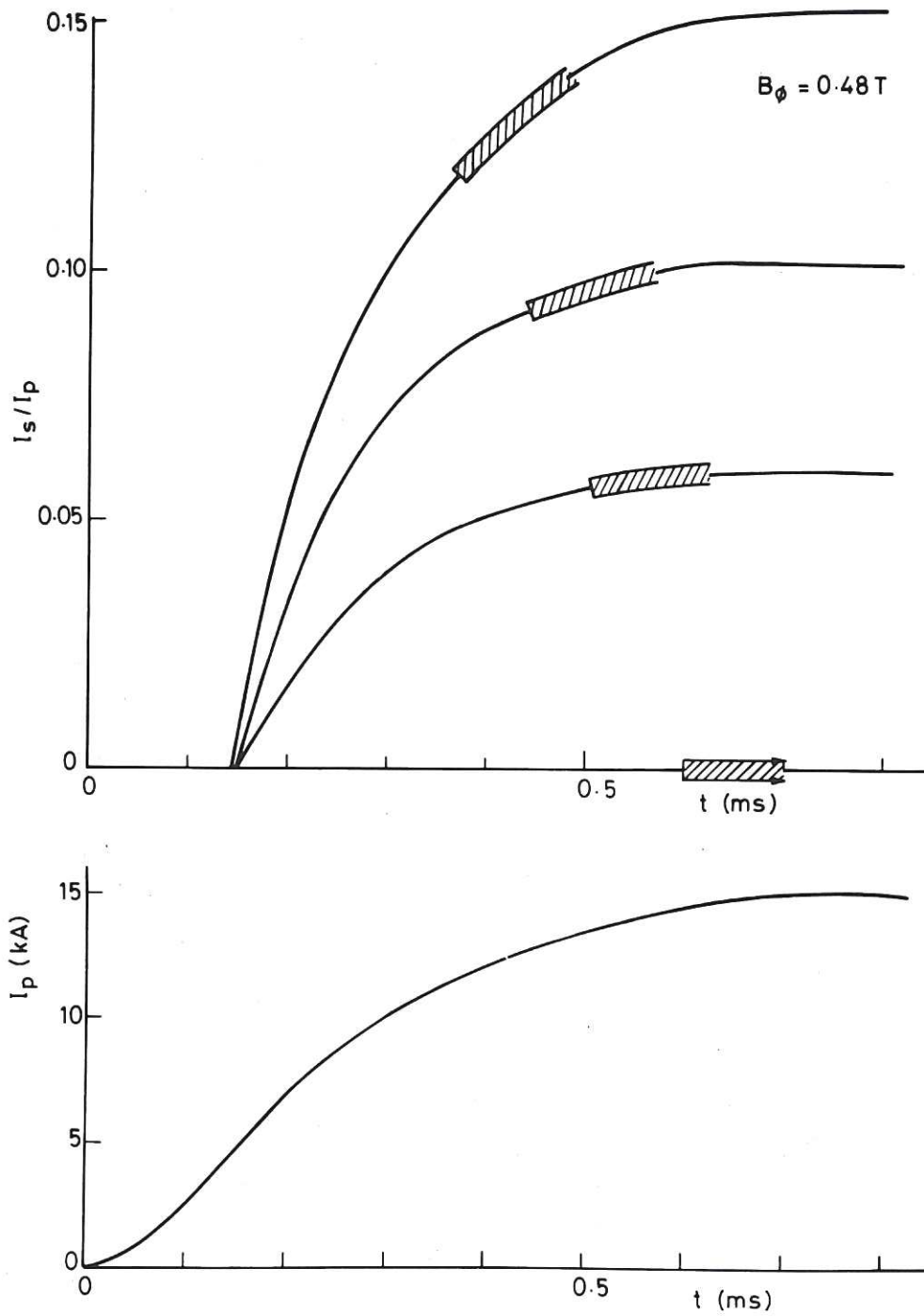


Fig.11 (a) The I_s/I_p trajectories for four different cases, with the toroidal field constant and the plasma current as shown in (b). The batching marks the start of the $m = 4, \ell = 1$ poloidal field oscillations.

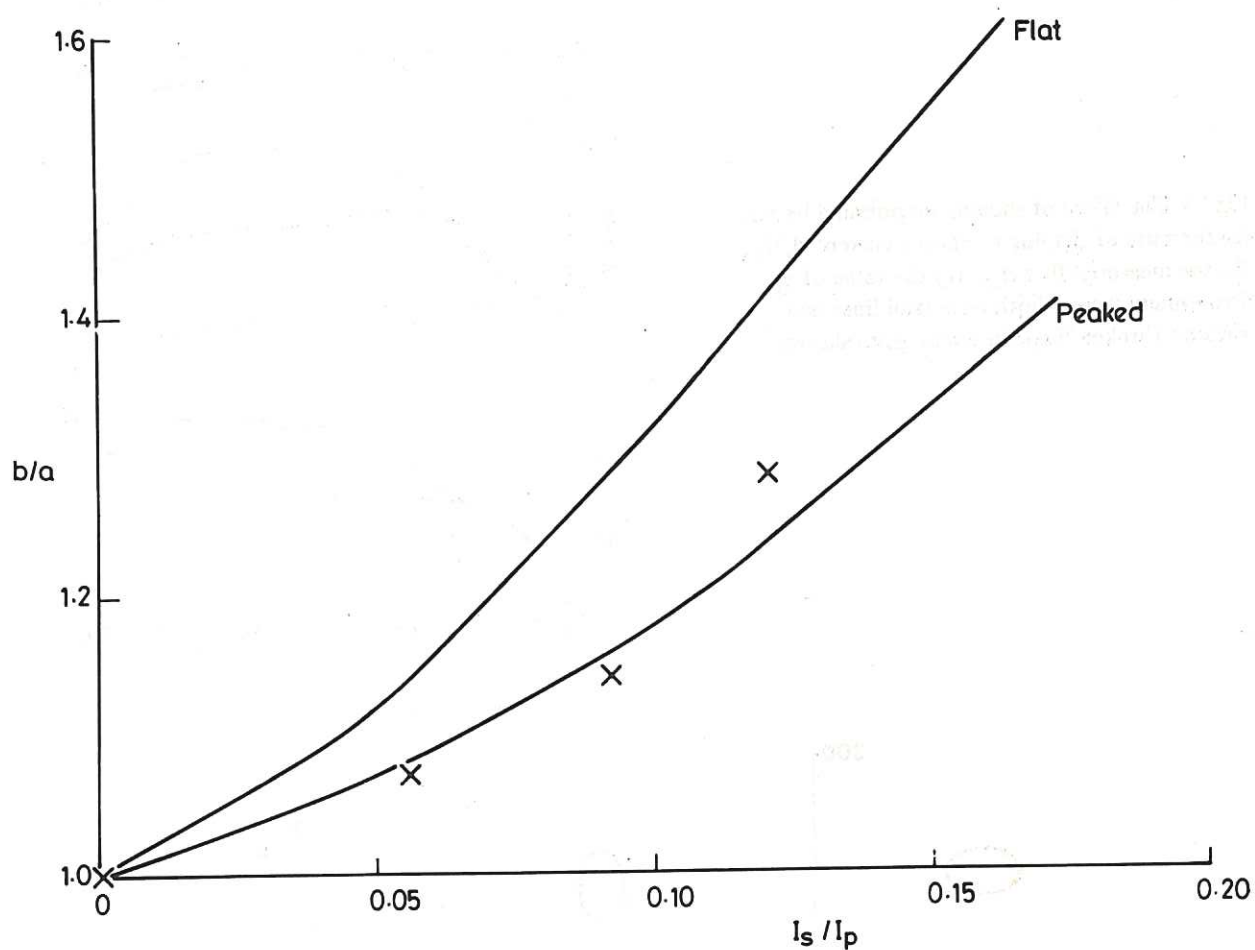


Fig.12 The semi axis ratio b/a deduced from the mode analysis, assuming $b = 8.5$ cm, as a function of the ratio I_s/I_p . Also shown are the curves resulting from the free boundary equilibrium analysis, with flat and peaked current distributions (Fig.5).

Fig.13 The effect of shaping on poloidal beta β_I :
 (a) the ratio of shaping to plasma current, I_s/I_p ;
 (b) the measured flux $\Delta\phi$; (c) the value of β_I .
 Experimental cases both with (full line) and
 without (broken line) the shaping are shown.

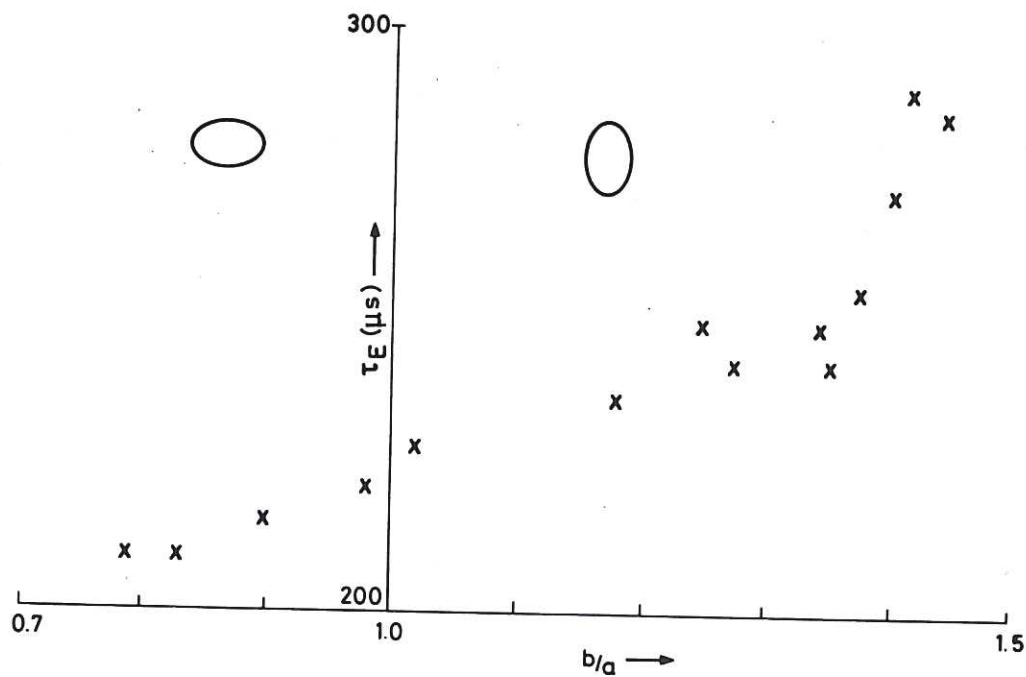
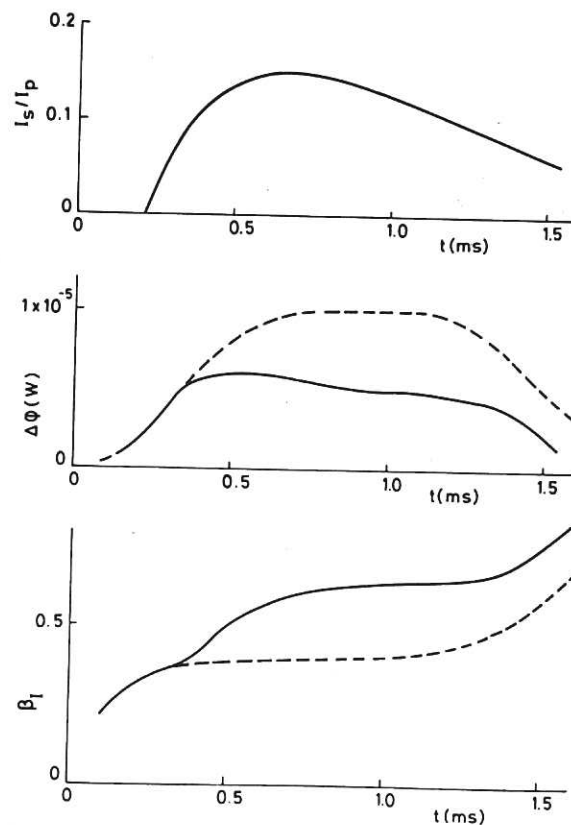


Fig.14 The measured confinement time τ_E , as a function of the semi axis ratio b/a . Results are shown for both vertical and horizontal ellipses.

